ISSN 1027-4510, Journal of Surface Investigation: X-ray, Synchrotron and Neutron Techniques, 2022, Vol. 16, No. 6, pp. 969–976. © Pleiades Publishing, Ltd., 2022.
Russian Text © The Author(s), 2022, published in Poverkhnost', 2022, No. 11, pp. 49–56.

Formation and Growth of Grain Boundary (αTi) Layers and Their Hardness in Ti–Cr Alloys

A. S. Gornakova[a], *, N. S. Afonikova[a], E. Yu. Postnova[a], A. N. Nekrasov[b], and B. B. Straumal[a], **

[a] *Osipyan Institute of Solid State Physics, Russian Academy of Sciences, Chernogolovka, 142432 Russia*

[b] *Korzhinskii Institute of Experimental Mineralogy, Russian Academy of Sciences, Chernogolovka, 142432 Russia*

**e-mail: alenahas@issp.ac.ru*

***e-mail: straumal@issp.ac.ru*

Received April 12, 2022; revised May 11, 2022; accepted May 11, 2022

Abstract—The structure of Ti–2 wt % Cr, Ti–4 wt % Cr, and Ti–5.5 wt % Cr alloys, annealed under conditions corresponding to the two-phase region (α + β) of the Ti–Cr phase diagram, is studied using scanning electron microscopy, X-ray diffraction analysis, and microindentation. The work studies the formation and growth of (αTi) phase layers at the grain boundaries (βTi)/(βTi). According to the results of X-ray diffraction analysis, all samples contain both (αTi) and (βTi) phases after annealing. For each alloy, the temperatures are determined at which continuous (αTi) phase layers are formed at the grain boundaries. The thickness and hardness of these layers are measured. The higher the chromium concentration, the harder are both the (αTi) and (βTi) phases. The (αTi)-phase hardness in the Ti–5.5 wt % Cr alloy is independent of the annealing temperature, but the (βTi)-phase hardness increases with decreasing annealing temperature.

Keywords: titanium, chromium, grain boundaries, grain-boundary wetting, hardness

DOI: 10.1134/S1027451022060106

INTRODUCTION

Titanium alloys have a wide range of applications in various industries [1–3]. Two-phase titanium alloys occupy a special place among them [4, 5]. A variation in their composition, as well as thermal and mechanical processing, enable one to control their properties, achieving the desired characteristics. Titanium alloys with the addition of up to 10 wt % of chromium belong to β-titanium alloys, which are attractive for biomedical applications, since they are characterized by a low Young's modulus close to the those values of natural bone [6–10].

The presence of two phases in the Ti–Cr system can lead to the appearance of grain-boundary wetting. This phenomenon is a process occurring upon heat treatment when the grain boundary (both grains belong to the same phase) is replaced by a layer of another phase different from the grain. As a result, two interphase boundaries are formed instead of one grain boundary. Grain-boundary wetting changes the physical and mechanical properties of a material. Phase transitions between complete and incomplete wetting in inmissible liquids were described for the first time in [11]. The authors predicted that in any two-phase mixture of liquids near their critical point, the contact angles with any third phase should become zero. Later [12, 13], the case was considered when a liquid droplet spreads over the surface. Two situations can arise depending on the value of the contact angle. If the contact angle is zero, wetting is complete and the droplet spreads over the surface. On the other hand, if the contact angle is between 0° and 180°, the droplet does not spread (this is the case of partial or incomplete wetting). The wetting transition is a surface phase transition from partial to complete wetting. The relationship between the wetting of grain boundaries in metals and the angle of their misorientation is described in detail, for example, for the Fe–30 wt % Mn–10 wt % Cu system [14]. The smaller the misorientation angle of grain boundaries, the more boundaries remain unwetted or dry. Detailed reviews on the wetting of grain boundaries by liquid and solid phases in multicomponent alloys are presented in [15–17]. The phase transformation of grain-boundary wetting can be of both the first and second order. The presence of such phase transformations was first observed in the Zn–Al system [18], and then in the Zn–Sn, Zn–In [19], and Zr–Nb [20] systems. The second (wetting) phase can be either liquid or solid. Several papers were published on the phenomenon of grain-boundary wetting by the second solid phase in binary titanium alloys, in which the microstructure of alloys with different concentrations of the second component (copper, cobalt, iron) preliminarily annealed under conditions corresponding to the two-phase region (α + β) phase diagrams [21–24]. The type of the second com-

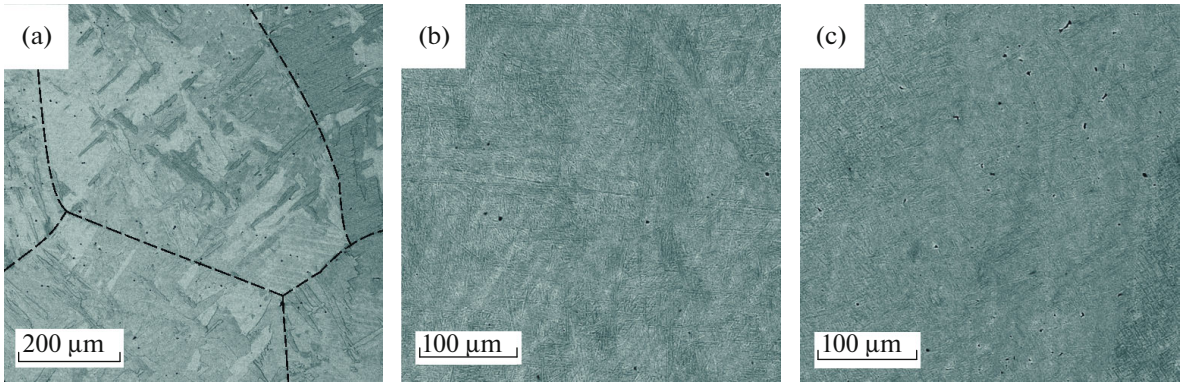

Fig. 1. SEM images of the cast alloys (a) Ti–2 wt % Cr, (b) Ti–4 wt % Cr, and (c) Ti–5.5 wt % Cr.

ponent and its amount significantly affect the wetting of grain boundaries. Therefore, the issue of wetting at grain boundaries, as well as the mechanical properties (for example, hardness) of the (αTi) and (βTi) phases in titanium alloys, is still relevant. The goal of this work is to study the wetting of grain boundaries in annealed Ti–Cr alloys from the two-phase region (α + β) of the Ti–Cr phase diagram and to measure the hardness of the (βTi) phase and (αTi) grain-boundary interlayers.

EXPERIMENTAL

We used two-component titanium alloys containing 2, 4, and 5.5 wt % of chromium ("in terms of charge"). The alloys were fabricated from titanium grade TI-1 with a purity of 99.98% and chromium with a purity of 99.99% by the method of levitation induction melting under argon. The component composition of all samples after smelting was determined using X-ray microanalysis (exact data on the composition according to the SEM results are given in parentheses): Ti–2 wt % Cr (Ti–2.09 ± 0.06 wt % Cr), Ti–4 wt % Cr (Ti–3.81 ± 0.08 wt % Cr), and Ti–5.5 wt % Cr (Ti–5.58 ± 0.15 wt % Cr).

Disks 2.0 mm in thickness were cut from the obtained cylindrical ingots with a diameter of 10.0 mm. Then, each sample was sealed into a quartz ampoule with a residual pressure of 4×10^{-4} Pa. The samples were annealed under conditions corresponding to the two-phase region (α + β) of the titanium-chromium state diagram: at 665°C (1032 h), 690°C (840 h), 730°C (768 h), 770°C (1200 h), and 810°C (720 h).

After quenching in water (together with the ampoule), the samples were sequentially ground on silicon-carbide grinding paper with a grain size of 220 to 2000 grit (grain size 68 and 10 μm, respectively), followed by polishing with diamond pastes with a grain size of 6, 3, and 1 μm. The structure of the polycrystalline samples was studied using a Neophot-32 optical microscope with a built-in Canon Digital Rebel XT 10 Mpix camera. For component analysis and imaging, we used Tescan Vega TS5130 MM Oxford Instruments and Supra 50VP scanning electron microscopes with an INCA Energy+ microanalysis system equipped with an Oxford Instruments energy-dispersive spectrometer. Phase analysis of the samples was performed by interpreting X-ray diffraction patterns obtained using a Siemens D-500 X-ray diffractometer using Cu$K_{\alpha 1}$ radiation. The microhardness was measured using a PMT-3 device with a Vickers indenter in the volume of (βTi) grains and at (αTi) grain-boundary layers. The microhardness measurements were carried out at a load of $P = 20$ g for the sample annealed at 690°C, and a load of $P = 50$ g for all other samples. The load value was selected depending on the thickness of the grain-boundary layer. Therefore, at a lower annealing temperature of 690°C, when the layer is thinner, the load on the indenter was smaller, also eliminating the effect of the (βTi)/(αTi) interfacial boundaries. The microhardness values were averaged over ten independent experiments for each phase.

RESULTS AND DISCUSSION

Structure and Phase Composition of the Initial Alloys

Figure 1 shows SEM images of the cast alloys (a) Ti–2 wt % Cr, (b) Ti–4 wt % Cr, and (c) Ti–5.5 wt % Cr, recorded in the backscattered electron mode. Since the phase contrast in cast alloys is weak, which can be easily explained by the uniform distribution of chromium in titanium after casting, as an example, we marked the grain boundaries in the Ti–2 wt % Cr alloy (Fig. 1a). The alloy is a polycrystal with coarse grains; there is no precipitation of the second phase (αTi) at the grain boundaries. The alloys under study contain two phases (Fig. 2), the portion of the (βTi) phase increases with increasing chromium concentration in the alloy (Table 1), and the lattice parameters of the (αTi) and (βTi) phases change insignificantly.

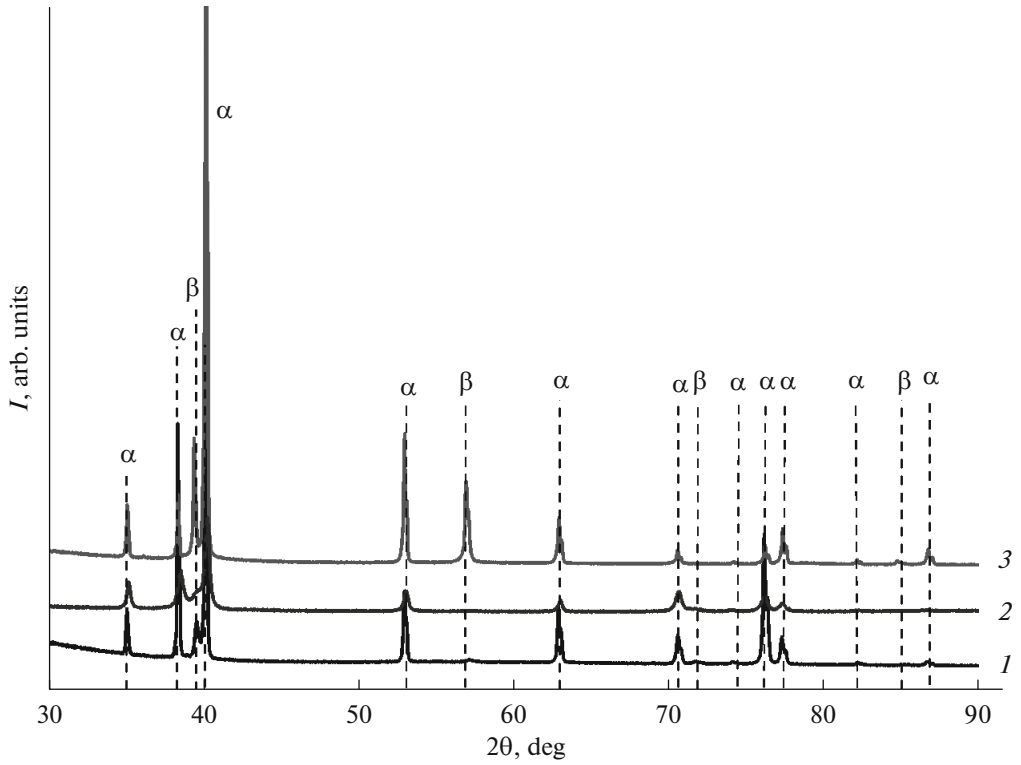

Fig. 2. X-ray diffraction patterns of the cast alloys (*1*) Ti–2 wt % Cr, (*2*) Ti–4 wt % Cr, and (*3*) Ti–5.5 wt % Cr.

Structure and Phase Composition of the Annealed Alloys

A series of SEM images (Fig. 3) demonstrates the dependence of the structure of the three investigated alloys on the annealing temperature. The samples consist of grains of the (βTi) phase and colonies of the (αTi) phase inside these grains. With an increase in temperature, these colonies are destroyed and form interlayers of the (αTi) phase at the (βTi)/(βTi) grain boundaries. (βTi)/(βTi) grain boundaries completely covered by the (αTi) phase first appear in the three studied alloys at different annealing temperatures.

Table 2 shows the results of X-ray diffraction analysis for the three annealed alloys at three different temperatures. Significant changes can only be observed in the lattice parameter *a* of the cubic (βTi) phase, in which *a* varies from a minimum value of 0.3220 nm to a maximum value of 0.3231 nm. The portion of the (βTi) phase in the samples increases with increasing chromium concentration, according to the phase diagram. The sample of Ti–5.5 wt % Cr alloy, annealed at 810°C, is highly textured and grains have an acicular shape. The lines of the (αTi) phase in the X-ray diffraction pattern are rather broadened at large reflection angles. All this indicates that the (αTi) phase is (α'Ti) martensite. Thus, the annealing conditions for this sample corresponded to the single-phase region (β) rather than the two-phase region (α + β) in the phase diagram. Quenching caused the formation of martensite in a Ti–5.5 wt % Cr sample, and grain-boundary wetting did not occur in it. This sample was not considered in further work.

To determine the component composition in the grain and the grain-boundary layer of the (αTi) phase, we performed chemical analysis across the (βTi)/(βTi) boundary in a Ti–5.5 wt % Cr sample annealed at 730°C (Fig. 4a). The grain-boundary layer of the (αTi) phase contains about 0.3 wt % of chromium (Fig. 4b). Figure 4c shows the temperature dependences of the average thickness of the grain boundary layer 2Δ in the

Table 1. Lattice parameters of the α and β phases and portion of the β phase in the cast alloys

Chromium concentration, wt %	Lattice parameters of the α phase, nm	Lattice parameters of the α phase, nm	Fraction of the β phase, %
2	$a = 0.2951$; $c = 0.4684$	$a = 0.3223$	8
4	$a = 0.2953$; $c = 0.4689$	$a = 0.3229$	13
5.5	$a = 0.2950$; $c = 0.4680$	$a = 0.3214$	34

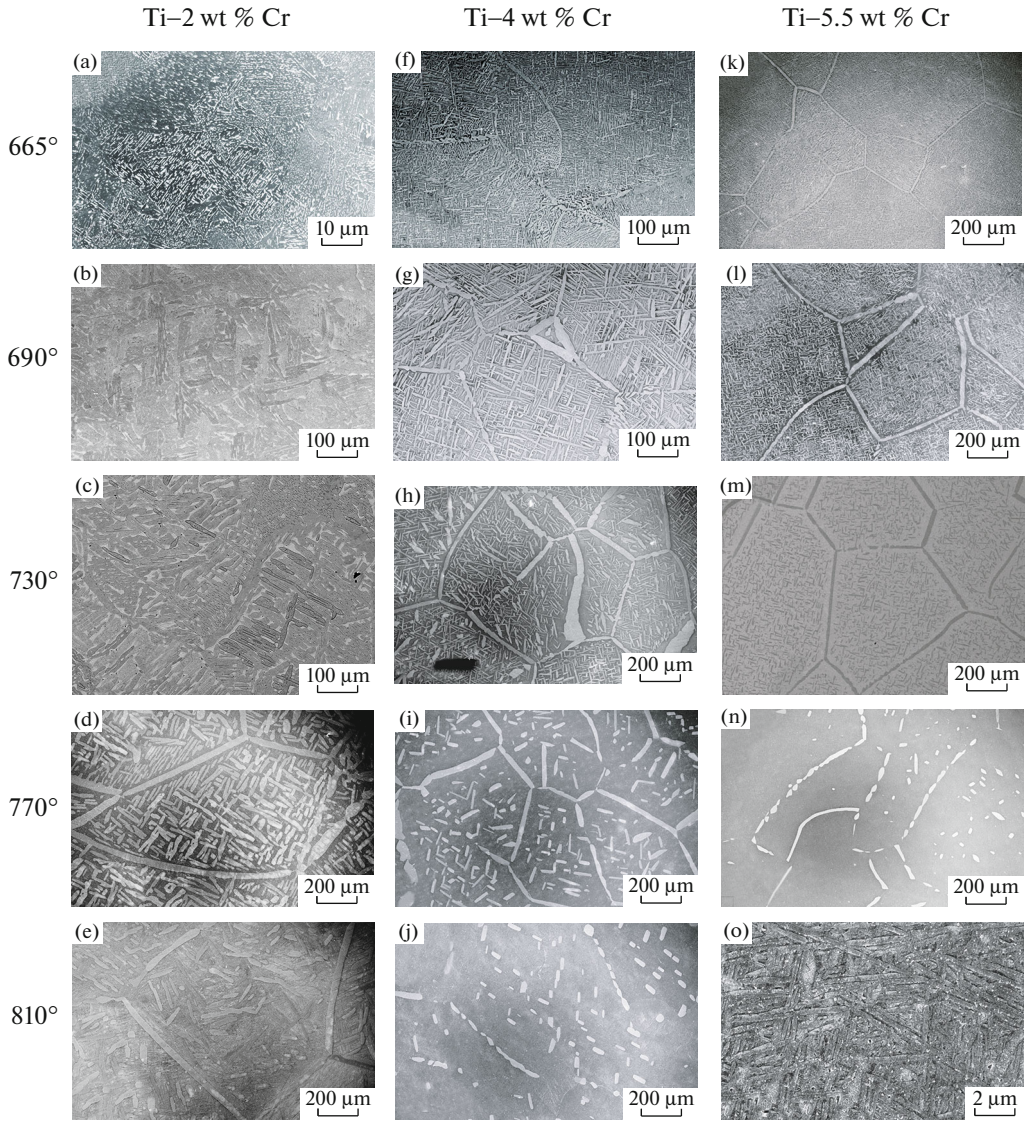

Fig. 3. SEM images of the cast alloys (a–e) Ti–2 wt % Cr, (f–j) Ti–4 wt % Cr, and (k–o) Ti–5.5 wt % Cr.

three investigated alloys. For the Ti–4 wt % Cr alloy, the average thickness of the grain-boundary (αTi) phase interlayer increases with an increase in the annealing temperature by a factor of 3. In Ti–2 wt % Cr and Ti–5.5 wt % Cr samples, the values of 2Δ decrease as they approach the transus line, that is, the boundaries of the β and α + β regions in the phase diagram. Figure 4d shows a slight increase in the average grain size with an increase in the annealing temperature in all samples.

Microhardness of the Annealed Alloys

In this work, we measured the microhardness of the grain-boundary (αTi) phase interlayers (dark gray areas in Fig. 4a) and grains (βTi) (light gray areas in Fig. 4a). The results of these measurements are presented in Fig. 5.

The values of the microhardness of the phases (αTi) and (βTi) for the three investigated alloys annealed at the same temperature of 770°C (1200 h) showed that an increase in the chromium concentration in the (αTi) and (βTi) solid solutions increases also the microhardness of (αTi) and (βTi) phases (Fig. 5a). According to the Ti–Cr phase diagram, at the same annealing temperature, the portion of phases in the alloys changes, while the composition of the phases should remain unchanged. Although the conditions for annealing and quenching of the alloys were the same, quenching has the main effect on the component composition of the phases: the portion of chromium in each phase in each alloy, the structure, morphology, and hence the microhardness of the phases.

Table 2. Lattice parameters of the (αTi) and (βTi) phases and their volume fraction in annealed alloys

Chromium concentration, wt %	T, °C	Lattice parameters of the α phase, nm	Lattice parameters of the α phase, nm	Volume fraction of the β phase, %
2	665	$a = 0.2949$; $c = 0.4690$	$a = 0.3229$	8
	730	$a = 0.2950$; $c = 0.4686$	$a = 0.3226$	1
	810	$a = 0.2949$; $c = 0.4685$	$a = 0.3225$	3
4	665	$a = 0.2950$; $c = 0.4688$	$a = 0.3230$	14
	730	$a = 0.2950$; $c = 0.4686$	$a = 0.3222$	8
	810	$a = 0.2950$; $c = 0.4686$	$a = 0.3225$	16
5.5	665	$a = 0.2949$; $c = 0.4689$	$a = 0.3231$	24
	730	$a = 0.2951$; $c = 0.4689$	$a = 0.3220$	18
	810	$a = 0.2950$; $c = 0.4686$	$a = 0.3226$	3

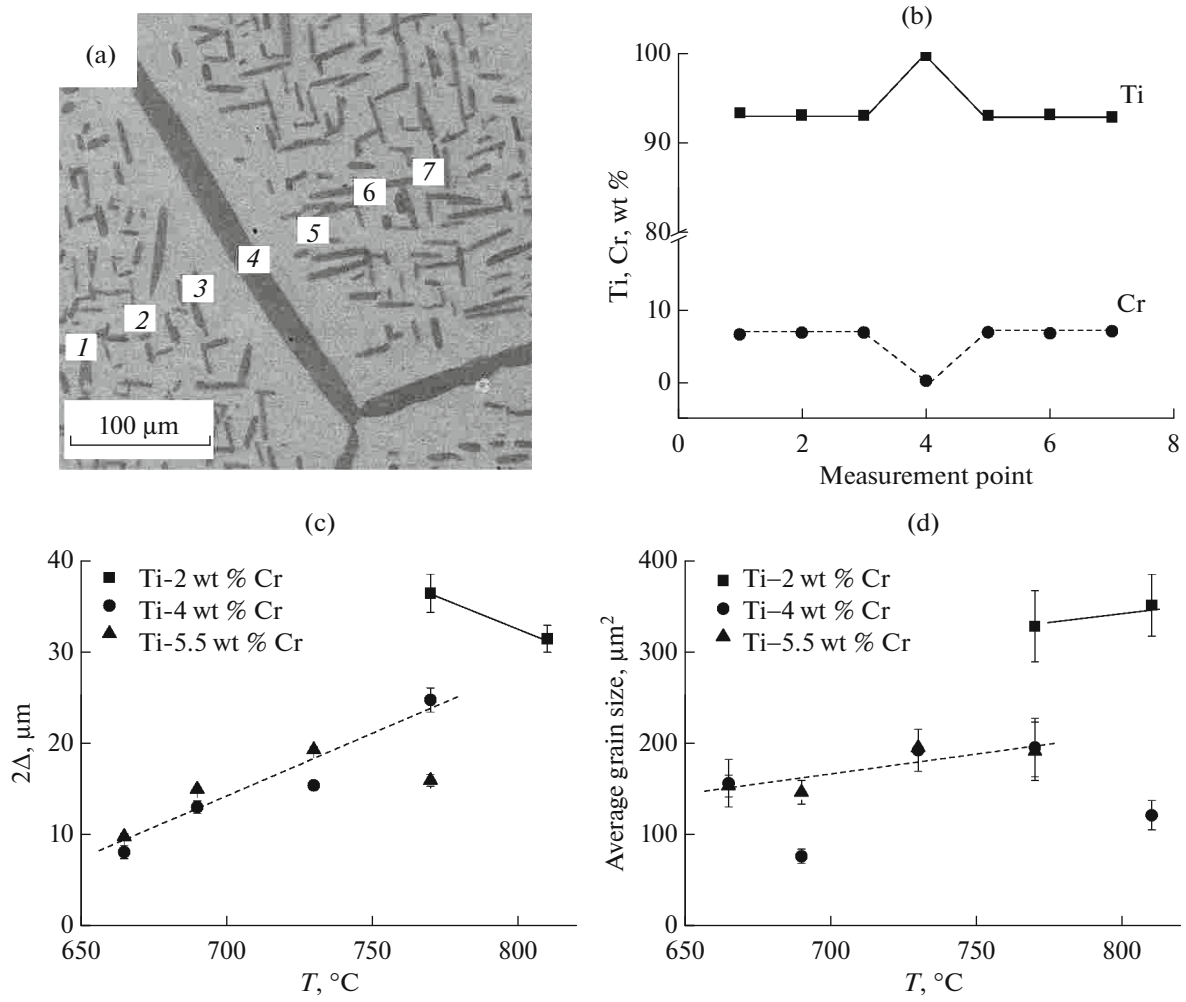

Fig. 4. (a) SEM image of the alloy Ti–5.5 wt % Cr annealed at 730°C: (dark gray areas) the (αTi) phase, (light gray areas) the (βTi) phase; (points 1–7) the areas of the sample in which the concentrations of titanium and chromium were determined (b). (c) Temperature dependences of the thickness of the grain-boundary layer 2Δ and (d) average grain size in Ti–2 wt % Cr, Ti–4 wt % Cr, and Ti–5.5 wt %Cr alloys.

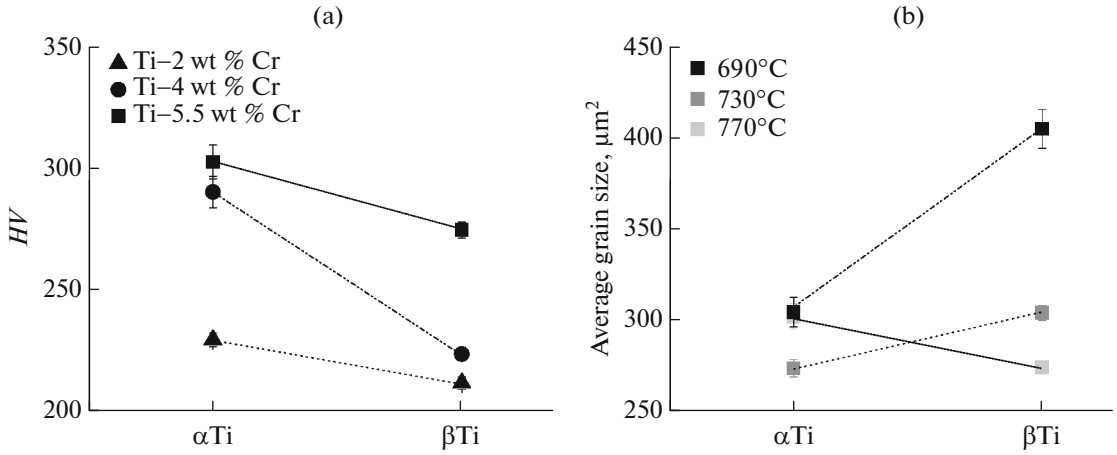

Fig. 5. Microhardness of the phases (αTi) and (βTi) (a) in Ti–2 wt % Cr, Ti–4 wt % Cr, and Ti–5.5 wt % Cr alloys annealed at 770°C (1200 h) and (b) in the Ti–5.5 wt % Cr alloy annealed at 690°C (840 h), 730°C (768 h), and 770°C (1200 h).

For the Ti–5.5 wt % Cr alloy (Fig. 5b) annealed at different temperatures, the microhardness values of the (αTi) phase vary from 270 to 300 *HV*, while for the (βTi) phase, they range from 270 to 400 *HV*. The microhardness of both phases increases with an increase in the annealing temperature. The solubility limit of chromium in (αTi) changes little with increasing temperature, so the microhardness also changes little. In this case, the composition of the (βTi) phase changes significantly. At an annealing temperature of 690°C (black areas in Fig. 5b), the chromium concentration in the solid solution (βTi,Cr) is ~9 wt %; at 730°C, it is ~7 wt % (dark gray areas); and at 770°C, it is ~5 wt % (light gray areas). Thus, by annealing under conditions corresponding to the two-phase region (αTi + βTi), and with a larger addition of chromium, one could increase the overall hardness of the material due to the formation of solid solution (βTi,Cr).

The morphology of the mutual arrangement of the phases was analyzed using a series of SEM images (Fig. 3). As an example, Fig. 6a shows the grain boundary (βTi)/(βTi) completely wetted by the (αTi) phase interlayer with the arrow (GB_w). The (βTi)/(βTi) grain boundary, which is not completely (partially) wetted by the (αTi) phase interlayer, is indicated as GB_{nw}. The temperature dependences of the fraction of grain boundaries (βTi)/ (βTi) completely wetted by the (αTi) phase interlayer for the three alloys studied are given in Fig. 6b.

At low concentrations of the second component (2 wt % Cr), the first grain boundaries (βTi)/(βTi) completely wetted by the (αTi) phase interlayer appear as the annealing temperature approaches the transus line, and their fraction changes abruptly from 0 to 80%. In the other two alloys, the portion of grain boundaries (βTi)/(βTi) completely wetted by the (αTi)-phase interlayers, on the contrary, decreases with increasing temperature. We failed to detect 100% wetting of grain boundaries (βTi)/(βTi) by the (αTi)-phase interlayers, as in [21–24]. This is probably due to the complex phase morphology in titanium alloys. In the as-cast state, grains of the (βTi) phase contain colonies of (αTi)-phase lamellae [4], and heat treatment of the alloy leads to coagulation of the lamellae and their growth. In addition, isolation at the grain boundaries, i.e., the formation of interlayers of the (αTi) phase along the grain boundaries occurs abruptly, and the thickness of the (αTi) grain-boundary layer can only be measured when it becomes noticeable by scanning microscopy. The maximum wetting of 80% is probably associated with the misorientation spectrum of grain boundaries, from low-angle to high-angle boundaries. Thus, Takashima et al. [14] studied the phenomenon of wetting of grain boundaries in the Fe–30% Mn–10% Cu alloy in detail and demonstrated that it is associated with grain misorientation, as was also shown for individual grain boundaries in the Zn–Al system [18]. Unfortunately, due to martensitic transformations in titanium, it is challenging to estimate the grain misorientation in polycrystalline titanium alloys even by electron backscatter diffraction. Glavicic et al. [25] developed a method for determining the orientation of the high-temperature β phase from the measured electron backscattering data for the low-temperature α phase in the Ti–6Al–4V alloy. Therefore, from the portion of completely wetted grain boundaries, one can indirectly estimate the portion of low- and high-angle grain boundaries (grain boundaries with a misorientation from 15° to 50° are wetted first) and evaluate the hardness of the material by the known composition of the alloy.

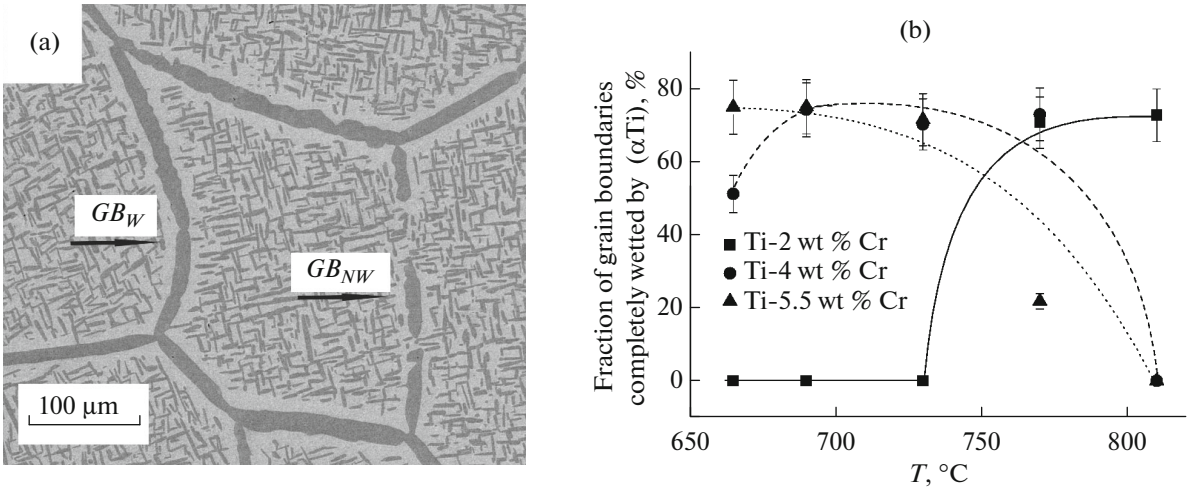

Fig. 6. (a) SEM image of the Ti–5.5 wt % Cr alloy annealed at 690°C: (dark gray areas) the (αTi) phase and (light gray areas) the (βTi) phase; (GB_w) is the (βTi)/(βTi) grain boundary completely wetted by the (αTi)phase interlayer; (GB_{nw}) is the (βTi)/(βTi) grain boundary incompletely (partially) wetted by the (αTi) phase interlayer. (b) Temperature dependence of the fraction of (βTi)/(βTi) grain boundaries completely wetted by the (αTi)-phase interlayer in Ti–2 wt % Cr, Ti–4 wt % Cr, and Ti–5.5 wt % Cr alloys.

CONCLUSIONS

The structure and morphology of Ti–2 wt % Cr, Ti–4 wt % Cr, and Ti–5.5 wt % Cr alloys, annealed under conditions corresponding to the two-phase region (α + β) of the Ti–Cr phase diagram, were studied. The average grain size was determined for each annealed sample; the largest grains ~350 μm in size were found in the alloy with 2 wt % of Cr. The thickness of the layers of the (αTi) phase at the grain boundaries (βTi)/(βTi) was measured; with an increase in the annealing temperature by ~100°C, it increases three times. The fraction of grain boundaries (βTi)/(βTi) completely covered (wetted) with (αTi)-phase interlayers was determined for each alloy at all annealing temperatures. The maximum fraction of completely wetted (βTi)/(βTi) grain boundaries is 80%. The Vickers hardness value of the (αTi) phase does not depend on the annealing temperature, but the lower the annealing temperature, the higher the (βTi) phase hardness. The larger the fraction of the second component in the alloy, the harder the (αTi) and (βTi) phases.

FUNDING

The work was supported by the Ministry of Science and Higher Education of the Russian Federation (agreement no. 075-15-2021-945, project no. in EB 13.2251.21.0013).

CONFLICT OF INTEREST

We declare that we have no conflicts of interest.

REFERENCES

1. U. Zwicker, *Titanium and Titanium Alloys* (Springer, Berlin, 1974).
2. G. Lütjering and J. C. Williams, *Titanium*, 2nd ed. (Springer, Berlin, 2007).
3. C. Veiga, J. P. Davim, and A. J. R. Loureiro, Rev. Adv. Mater. Sci. **32**, 133 (2012).
4. J. Chrapoński and W. Szkliniarz, Mater. Charact. **46**, 149 (2001). http://www.doi.org/10.1016/S1044-5803(01)00117-6
5. S. A. Salihu and I. Y. Suleiman, IOSR J. Appl. Phys. **11**, 35 (2019). http://www.doi.org/10.9790/4861-1102013539
6. Yu. Shinohara, T. Ishigaki, T. Inamura, H. Kanetaka, Sh. Miyazaki, and H. Hosoda, Mater. Sci. Forum **654–656**, 2122 (2010). http://www.doi.org/10.4028/www.scientific.net/MSF.654-656.2122
7. Y. Kusano, T. Inamura, H. Hosoda, K. Wakashima, and S. Miyazaki, Adv. Mater. Res. **89–91**, 307 (2010). http://www.doi.org/10.4028/www.scientific.net/AMR.89-91.307
8. F. V. Kiryukhantsev-Korneev, A. N. Sheveiko, V. A. Komarov, M. S. Blanter, E. A. Skryleva, N. A. Shirmanov, E. A. Levashov, and D. V. Shtansky, Russ. J. Non-Ferrous Met. **52**, 311 (2011). http://www.doi.org/10.3103/S1067821211030138
9. Y. Murayama, Sh. Sasaki, H. Kimura, and A. Chiba, Mater. Sci. Forum. **638–642**, 635 (2010). http://www.doi.org/10.4028/www.scientific.net/MSF.638-642.635
10. M. Nakai, M. Niinomi, J. Hieda, and T. Shibata, ISIJ Int. **52**, 1655 (2012). http://www.doi.org/10.2355/isijinternational.52.1655
11. J. W. Cahn, J. Chem. Phys. **66**, 3667 (1977). http://www.doi.org/10.1063/1.434402

12. D. Bonn and D. Ross, Rep. Prog. Phys. **64**, 1085 (2001). http://www.doi.org/10.1088/0034-4885/64/9/202
13. D. Bonn, D. Ross, E. Bertrand, K. Ragil, N. Shahidzadeh, D. Broseta, and J. Meunier, Phys. A (Amsterdam, Neth.) **306**, 279 (2002). http://www.doi.org/10.1016/S0378-4371(02)00505-8
14. M. Takashima, P. Wynblatt, and B. L. Adams, Interface Sci. **8**, 351 (2000). http://www.doi.org/10.1023/A:1008727728076
15. B. B. Straumal, A. Korneva, G. A. Lopez, A. Kuzmin, E. Rabkin, G. Gerstein, A. B. Straumal, and A. S. Gornakova, Materials **14**, 7506 (2021). http://www.doi.org/10.3390/ma14247506
16. B. B. Straumal, A. Korneva, A. Kuzmin, G. A. Lopez, E. Rabkin, A. B. Straumal, G. Gerstein, and A. S. Gornakova, Metals **11**, 1881 (2021). http://www.doi.org/0.3390/met11111881
17. B. Straumal, E. Rabkin, G. A. Lopez, A. Korneva, A. Kuzmin, A. Gornakova, A. Straumal, and B. Baretzky, Crystals **11**, 1540 (2021). http://www.doi.org/10.3390/cryst11121540
18. B. B. Straumal, A. S. Gornakova, O. A. Kogtenkova, and S. G. Protasova, Phys. Rev. B **78**, 054202 (2008). http://www.doi.org/10.1103/PhysRevB.78.054202
19. A. S. Gornakova, B. B. Straumal, S. Tsurekawa, L.-S. Chang, and A. N. Nekrasov, Rev. Adv. Mater. Sci. **21**, 18 (2009).
20. B. B. Straumal, A. S. Gornakova, Y. O. Kucheev, B. Baretzky, and A. N. Nekrasov, J. Mater. Eng. Perform. **21**, 721 (2012). http://www.doi.org/10.1007/s11665-012-0158
21. A. S. Gornakova, S. I. Prokofiev, B. B. Straumal, and K. I. Kolesnikova, Russ. J. Non-Ferrous Met. **57**, 703 (2016). http://www.doi.org/10.3103/S1067821216070099
22. B. B. Straumal, A. S. Gornakova, S. I. Prokofjev, N. S. Afonikova, B. Baretzky, A. N. Nekrasov, and K. I. Kolesnikova, J. Mater. Eng. Perform. **23**, 1580 (2014). http://www.doi.org/10.1007/s11665-013-0789-3
23. A. S. Gornakova, B. B. Straumal, A. N. Nekrasov, A. Kilmametov, and N. S. Afonikova, J. Mater. Eng. Perform. **27**, 4989 (2018). http://www.doi.org/10.1007/s11665-018-3300-3
24. A. S. Gornakova, S. I. Prokofiev, K. I. Kolesnikova, and B. B. Straumal, Russ. J. Non-Ferrous Met. **57**, 229 (2016). http://www.doi.org/10.3103/S106782121603007X
25. M. G. Glavicic, P. A. Kobryn, T. R. Bieler, and S. L. Semiatin, Mater. Sci. Eng., A **346**, 50 (2003). http://www.doi.org/10.1016/S0921-5093(02)00535-X

Translated by O. Zhukova